


Spin and charge fluctuation induced pairing in ABCB tetralayer graphene

Ammon Fischer^{1,*}, Lennart Klebl^{2,*}, Jonas B. Profe¹, Alexander Rothstein^{3,4}, Lutz Waldecker^{1,3}, Bernd Beschoten³, Tim O. Wehling^{2,5} and Dante M. Kennes^{1,6,†}¹*Institute for Theory of Statistical Physics, RWTH Aachen University, and JARA Fundamentals of Future Information Technology, 52062 Aachen, Germany*²*I. Institute for Theoretical Physics, Universität Hamburg, Notkestraße 9-11, 22607 Hamburg, Germany*³*2nd Institute of Physics and JARA-FIT, RWTH Aachen University, 52074 Aachen, Germany*⁴*Peter Grünberg Institute (PGI-9), Forschungszentrum Jülich, 52425 Jülich, Germany*⁵*The Hamburg Centre for Ultrafast Imaging, 22761 Hamburg, Germany*⁶*Max Planck Institute for the Structure and Dynamics of Matter, Center for Free Electron Laser Science, 22761 Hamburg, Germany* (Received 6 June 2023; revised 18 August 2023; accepted 25 October 2023; published 8 January 2024)

Motivated by the recent experimental realization of ABCB stacked tetralayer graphene [Wirth *et al.*, *ACS Nano* **16**, 16617 (2022)], we study correlated phenomena in moiré-less graphene tetralayers for realistic interaction profiles using an orbital resolved random phase approximation approach. We demonstrate that magnetic fluctuations originating from local interactions are crucial close to the van Hove singularities on the electron- and hole-doped side promoting layer selective ferrimagnetic states. Spin fluctuations around these magnetic states enhance unconventional spin-triplet, valley-singlet superconductivity with f -wave symmetry due to intervalley scattering. Charge fluctuations arising from long range Coulomb interactions promote doubly degenerate p -wave superconductivity close to the van Hove singularities. At the conduction band edge of ABCB graphene, we find that both spin and charge fluctuations drive f -wave superconductivity. Our analysis suggests a strong competition between superconducting states emerging from long- and short-ranged Coulomb interactions and thus stresses the importance of microscopically derived interaction profiles to make reliable predictions for the origin of superconductivity in graphene-based heterostructures.

DOI: [10.1103/PhysRevResearch.6.L012003](https://doi.org/10.1103/PhysRevResearch.6.L012003)

Introduction. The experimental discovery of cascades of correlated phases and superconductivity in ultraclean graphene multilayers without [1–6] and with [7–19] a stacking twist has led to tremendous research interest. Experimental studies of multilayer graphene suggest the existence of ferromagnetic phases in the form of half- and quarter metals [1,20], Wigner crystals [1], and in particular superconductivity that emerges in Bernal bilayer (AB) and rhombohedral trilayer (ABC) graphene for external displacement fields and either in the presence of external magnetic fields [2,4] or proximity induced spin-orbit coupling [3,5]. From a fabrication point of view, untwisted graphene stacks are simpler to handle as twist angle variations and other stacking imperfections are easier to control. It is therefore that experiments along with atomistic theoretical studies can provide a microscopic understanding of correlation effects, in particular as hindering disorder effects can be disregarded and multilayer graphene stacks omit nm-scale unit cells as well as a more sophisticated theory of

topological obstruction of the low-energy bands when compared to their twisted counterparts [21–23].

Nonetheless, band flattening in untwisted graphene stacks is restricted to small Fermi surface patches around the valleys K and K' , which hampers theoretical descriptions without losing contact to the microscopics. Previous works [24–36] resort to effective continuum or adapted Slonczewski-Weiss-McClure models with ultraviolet cutoff that are only valid near the valleys $K^{(\prime)}$ and hence severely complicate a description of realistic orbital-resolved interaction profiles that account for short- and long-ranged interactions consistently. Instead, an approximate spin/valley $SU(4)$ symmetry arises from considering the long-ranged tail of the Coulomb interaction alone.

Motivated by the recent experimental characterization of different tetralayer graphene stacks [37,38], we remedy the aforementioned shortcomings and study correlated phenomena in moiré-less graphene tetralayers for *ab initio* motivated models and realistic interaction profiles using an orbital resolved random phase approximation approach (RPA). In particular, we focus on ABCB stacked graphene that breaks inversion symmetry and thus features intrinsic electrical fields. The latter open a band gap at charge neutrality and hence play the same role as external displacement fields that are necessary to stabilize superconductivity in bi- and trilayer graphene. While previous works mainly focused on pairing mediated by electron-phonon coupling [39–41], fluctuations around flavor symmetry broken phases [24–27], or charge fluctuations arising from repulsive Coulomb

*These authors contributed equally to this work.

†dante.kennes@mpsd.mpg.de

interactions [28–36], we discuss the interplay of spin and charge fluctuations to the formation of weak coupling instabilities on general grounds based on a microscopic model of the carbon p_z orbitals. In view of the various spin-polarized phases governing large areas of the phase diagram of bi- and trilayer graphene [1], we first characterize the role of spin fluctuations towards the formation of magnetic order in ABCB graphene. To disentangle the influence of long- and short-ranged interactions as well as their contributions to spin- and charge-enhanced superconductivity, we next study three different pairing mechanisms based on (i) spin-fluctuations from local interactions (x RPA) (ii) screening of long-ranged Coulomb interactions (d RPA) and (iii) a combined approach (x d RPA) that captures both long- and short-ranged Coulomb interactions.

Microscopic Model. We model the electronic band structure of graphene tetralayers employing a modified Slonczewski-Weiss-McClure Hamiltonian [42]. The resulting kinetic Hamiltonian represents an atomistic model of tetralayer graphene consistent with first-principle calculations [43], see Supplemental Material (SM) [44] for details on the parametrization. The upper panels of Fig. 1 show the low-energy band structure of the three inequivalent thermally stable stacking configurations of tetralayer graphene: ABCB (a), ABCA (b), and ABAB (c). The color encodes the polarization \mathcal{P}_o of the dominant orbitals. For ABCB graphene we find that most weight is concentrated on the a site in the first layer and the b site in the third layer. Due to broken layer inversion symmetry, ABCB graphene features a band gap of $\Delta_g \approx 20$ meV at charge neutrality without the application of an external electric field [45–47]. The latter can be explained by localization of charge carriers in the A and C layers creating a crystal field pointing from the outer B to the A layer. Due to this internally existing electric field, the bands become gapped at charge neutrality and experience additional flattening around the K and K' valleys. This is reflected in the density of states (DOS) [see Fig. 1(d)] that indicates van Hove singularities (VHS) close to charge neutrality on the electron- and hole-doped side. In particular, the internal electrical fields in ABCB boost the VHS compared to ABCA and ABAB graphene. Therefore, we expect the effects of electron-electron interactions to be most significant in ABCB graphene. By inspection of the ABCB Fermi surface for various fillings we observe a Lifshitz transition from a (annular) single-pocket to a three-pocket structure, which signals an intriguing interplay between nesting- and DOS-driven Fermi surface instabilities and resembles AB graphene under an electrical field. As the latter hosts magnetic states [1], we start with a discussion of spin fluctuation induced instabilities in the following.

Spin fluctuations and magnetic instabilities. To study magnetic correlations in few-layer graphene, we use a random phase approximation (RPA) approach. We calculate the free electronic susceptibility $\hat{\chi}_0(\mathbf{q}) = \text{Tr}_k[\hat{G}_0(k - \mathbf{q})\hat{G}_0^\dagger(k)]$ in the static limit $iq_0 \rightarrow 0$, where $\hat{G}_0(k)$ is the free Matsubara Green's function and $k = (ik_0, \mathbf{k})$ the electronic “four momentum.” The system's multiorbital nature is encoded in the (Hermitian) matrix structure of $\hat{\chi}_0(\mathbf{q})$, intrinsically rendering its components complex even in the static limit. Assuming a local Hubbard interaction U allows us to resum the infinite ladder series in the crossed particle-hole channel to

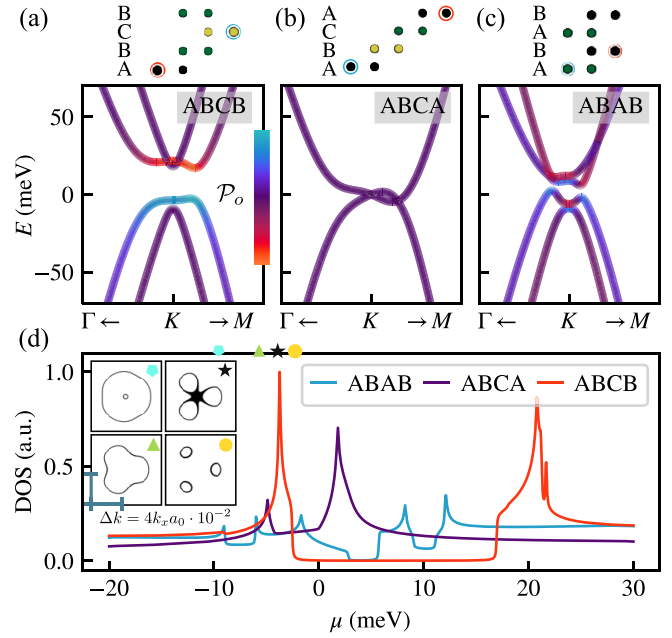


FIG. 1. Band structure and density of states (DOS) for different tetralayer graphene structures without an applied electric field. Panels (a)–(c): Low-energy band structure near valley K with the relative orbital polarization \mathcal{P}_o of the bands indicated by the diverging colormap. The different stacking configurations of ABCB, ABCA, and ABAB tetralayer graphene are shown above while the two sites with dominant spectral weight are indicated. Panel (d): DOS within the range of the valley-flat bands. Intrinsic electrical fields caused by broken inversion symmetry open a band gap of $\Delta_g \approx 20$ meV in ABCB stacked graphene and flatten the low-energy bands around the valleys K, K' . Hence, ABCB has the highest DOS near the van Hove singularities (VHS) on the electron- and hole-doped side. The inset highlights different Fermi surfaces around valley K as the chemical potential is tuned through the VHS on the hole-doped side. Starting from the edge of the valence band, the Fermi surface undergoes a Lifshitz transition as the three pockets originating from trigonal warping continuously transform to an annular Fermi surface.

arrive at a Stoner-like criterion [48] for the orbital-resolved susceptibility $\hat{\chi}_0(\mathbf{q})$: The critical interaction strength required for the onset of magnetic order is given by $U_c = 1/\chi_0^m(\mathbf{q}^m)$, with $\chi_0^m(\mathbf{q}^m)$ the largest (real) eigenvalue of $\hat{\chi}_0(\mathbf{q}^m)$ and \mathbf{q}^m the transfer momentum at which the maximum occurs. We adapt $T = 5 \cdot 10^{-5}$ eV as temperature broadening for $\hat{\chi}_0(\mathbf{q})$ throughout this work, see SM [44] for more details on the orbital-space RPA.

The assumption of starting from local Hubbard- U interactions is motivated by the substantial role screening plays in the vicinity of the VHS. Charge fluctuations predominantly suppress the long-wavelength component ($\mathbf{q} = 0$) of the initial Coulomb interaction at the VHS as mandated by the maximum of the polarization function $\hat{\chi}^0(\mathbf{q})$ at Γ , see Fig. 2(c). Contrarily, the effective RPA-renormalized interaction in the exchange channel $\hat{W}^{\text{RPA}}(\mathbf{q}) = \hat{U}[1 - \hat{U}\hat{\chi}_0(\mathbf{q})]^{-1}$ undergoes significant enhancement at Γ when resumming the remaining local interactions, see Fig. S3(r) in the Supplemental Material [44]. This aligns with recent experimental [1,4] and theoretical works [24–26,49] that report spin-polarized half metals in

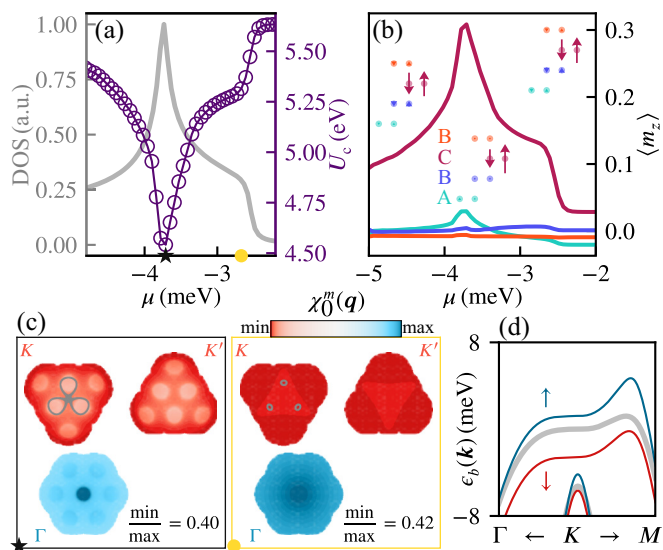


FIG. 2. Spin correlations in the presence of local interactions in ABCB tetralayer graphene. (a) Critical onsite interaction U_c required for the onset of magnetic order (purple) and DOS (grey) for μ close to the VHS of the valence band. We expect an increased tendency towards magnetic order at the van Hove filling $\mu_{\text{VHS}} \approx -3.9$ meV. The leading magnetic correlations are displayed in panel (b): Each curve corresponds to the magnetization within one layer. At $\mu \approx \mu_{\text{VHS}}$, local interactions drive ferrimagnetism in the C layer, while away from the VHS antiferromagnetic fluctuations gain importance in all layers. (c) Momentum structure of the leading eigenvalue of the susceptibility matrix $\hat{\chi}_0(\mathbf{q})$ for $\mu \approx \mu_{\text{VHS}}$ and $\mu > \mu_{\text{VHS}}$ [c.f. markers in (a)]. The transfer momenta supported by the Fermi surface are $\mathbf{q} \approx \Gamma$ and $\mathbf{q} \approx K^{(i)}$. The K valley (left subpanel) includes the Fermi contour. (d) Band renormalization of up (blue) and down (red) electrons due to the ferrimagnetic instability at μ_{VHS} .

related bi- and trilayer graphene structures near the VHS. For light hole doping, delocalization of the free electrons alongside the decreasing impact of electron screening suggests the revival of long-ranged Coulomb interactions. As a first step, we therefore focus on initial short-ranged interactions in the following and analyze its impact on magnetic ordering near the VHS.

Figure 2(a) demonstrates the magnetic ordering tendencies of ABCB tetralayer graphene near the valence band VHS for local interactions U . The critical interaction strength drops to $U_c \approx 4.5$ eV, which is of similar order as estimates of the effective (screened) onsite U in graphene [50,51]. In Fig. 2(b) we demonstrate that the valence band VHS drives ferrimagnetic fluctuations within the C layer of ABCB graphene, while away from the VHS layer-agnostic antiferromagnetic fluctuations gain in importance. The momentum structure of the magnetic susceptibility near $\mathbf{q} \approx \Gamma, K^{(i)}$ is shown in panel (c). The weight distribution of $\chi_0^m(\mathbf{q})$ evolves upon doping across the valence band VHS, but the leading contribution always stems from momenta close to Γ . To study band renormalization within the ferrimagnetic phase at the VHS, we post-process our RPA results within a self-consistent Hartree-Fock approach, see Fig. 2(d). The ferrimagnetic instability splits the band of spin up (down) electrons within both valleys equally and hence breaks the original spin

degeneracy of the system. Therefore, we conclude that exchange scatterings as represented by the Hubbard- U term are particularly relevant at the VHS driving ferrimagnetic order [52,53], which aligns with previous reports of spin-polarized half-metal phases [24–26,49] in other multilayer graphene stacks. Other orders, e.g., intervalley coherent order, may emerge as subsequent instabilities from the magnetic one in the presence of purely local interactions. For the VHS on the electron-doped side, a similar picture of magnetic instabilities emerges (see SM [44]), allowing us to focus on the hole-doped side.

Pairing from local interactions. As established in the previous paragraph, local interactions cause ferrimagnetic correlations to prevail in ABCB graphene on the hole-doped side. This is particularly striking as large areas in the phase diagram of bilayer graphene are governed by symmetry-broken phases that show clear indications of hysteresis [1]. Close to the ferrimagnetic instability, spin fluctuations arising from local, repulsive interactions can provide the pairing glue for an unconventional superconducting state [54–59], which is captured by the (static) pairing vertex

$$V_X^{\text{PP}}(\mathbf{k}, \mathbf{k}') = \hat{U} - \frac{\hat{U} \hat{\chi}_0(\mathbf{q}_X) \hat{U}}{1 - \hat{U} \hat{\chi}_0(\mathbf{q}_X)} + \frac{[\hat{U} \hat{\chi}_0(\mathbf{q}_D)]^2 \hat{U}}{1 - [\hat{U} \hat{\chi}_0(\mathbf{q}_D)]^2}, \quad (1)$$

where U is the local onsite interaction and $\mathbf{q}_{X(D)} = \mathbf{k} \pm \mathbf{k}'$ denotes the dominant momentum transfer in the exchange (direct) particle-hole channel, see SM [44] for details. We finally solve the linearized gap equation in the projected subspace containing the bands in an energy window W around the Fermi level

$$\lambda_{\text{SC}} \Delta_b(\mathbf{k}) = -\frac{1}{N_k} \sum_{\mathbf{k}'} \hat{V}_{S,bb'}^{\text{PP}}(\mathbf{k}, \mathbf{k}') \chi_{b'}^{\text{PP}}(\mathbf{k}') \Delta_{b'}(\mathbf{k}'), \quad (2)$$

where $\hat{V}_{S,bb'}^{\text{PP}}$ and $\chi_{b'}^{\text{PP}}$ denote the band-projected effective pairing vertex and particle-particle susceptibility, respectively. The largest coupling constant is proportional to the critical temperature $T_c = T e^{-1/\lambda_{\text{SC}}}$ of the superconducting transition [60] and the corresponding eigenfunction yields the symmetry of the superconducting (SC) order parameter $\Delta_b(\mathbf{k})$.

Since local interactions are flat in momentum space, they induce both inter- and intravalley coupling. In conjunction with single layer ferromagnetic fluctuations, the intervalley exchange enhances order parameters that are (i) spin-triplet and (ii) change sign under a valley flip. We find that local interactions (x RPA) exclusively promote valley-singlet, spin-triplet f -wave order for all fillings around the VHS in ABCB stacked graphene. The coupling constant λ_{SC} is enhanced close to the Stoner transition for $U = 4$ eV as plotted in purple in Fig. 3(a), while it decreases continuously when doping away from the VHS. As soon as the Stoner regime is reached ($U \geq U_c$), superconductivity is suppressed and the peak of the coupling constant λ_{SC} splits into two as shown in Fig. 3(b). Further screening of local interactions may therefore shift the position of superconducting regions observed in experiment [11].

Pairing from screened Coulomb interactions. Screened Coulomb repulsion was discussed to provide the dominant pairing glue in bi- and trilayer graphene [28–31,34,61]. In

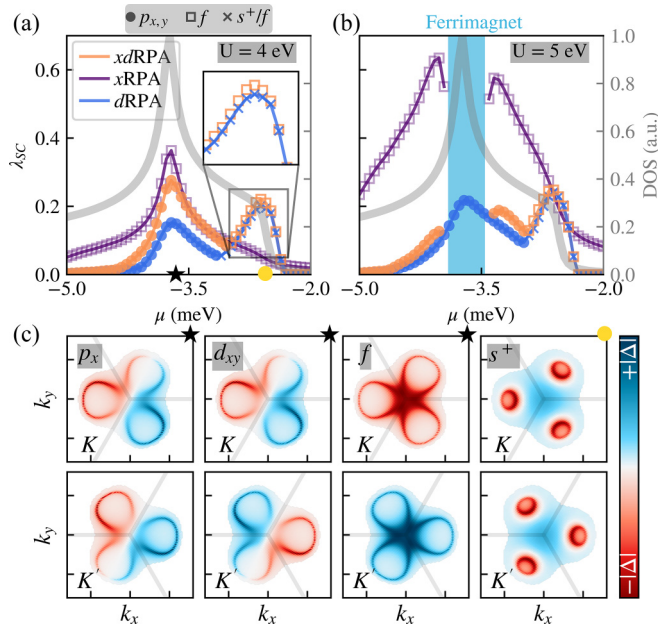


FIG. 3. Superconducting instabilities mediated by spin and charge fluctuations in ABCB graphene. (a),(b) Leading SC coupling constant λ_{SC} as function of the chemical potential μ for different values of the onsite interaction U . Screening ($dRPA$) favors doubly-degenerate $p_{x,y}$ -wave superconducting order near the VHS (black star) and almost degenerate f/s^+ -wave SC order for low-hole doping (yellow circle). Spin exchange ($xRPA$) exclusively enhances spin-triplet f -wave superconductivity around the Stoner transition, until ferrimagnetic order eventually displaces SC at the VHS for $U \gtrsim U_c$ (b). Combining the effect of spin and charge fluctuations ($xdRPA$) enhances screening driven spin-triplet SC order near the Stoner instability hinting towards significant screening of local interactions by charge fluctuations. The corresponding SC order parameters in the valleys K and K' are displayed in (c).

the continuum theories employed by a majority of works, the additional flavor degeneracy due to the valley degree of freedom enhances the polarization function $\chi_0(\mathbf{q})$ by a factor of 4 instead of 2 compared to the usual spin $SU(2)$, which boosts the contribution of charge fluctuations to electron-mediated pairing. However, effective continuum theories hinder a direct description of the microscopic interaction containing long- and short-ranged terms. This manifests in an effective spin/valley $SU(4)$ symmetry that must be lifted by a (phenomenological) intervalley Hund's coupling [34,61]. Here, we remedy this shortcoming by exploiting the orbital-resolved RPA approach presented in this manuscript and use the ‘‘Ohno’’ interaction profile [50,62]

$$V^O(\mathbf{r}) = \frac{Ua}{\sqrt{a^2 + \mathbf{r}^2}} e^{-r/d}, \quad (3)$$

where we set $a = 0.3a_0$, $d = 200a_0$, and $a_0 = 2.46 \text{ \AA}$ motivated by first-principle calculations [50,51]. Pairing due to interaction-induced screening is captured by the effective vertex

$$\hat{V}_D^{PP}(\mathbf{k}, \mathbf{k}') = \frac{\hat{V}^O(\mathbf{q}_D)}{\mathbb{1} + 2\hat{V}^O(\mathbf{q}_D)\hat{\chi}_0(\mathbf{q}_D)} \delta_{\mathbf{q}_D, \mathbf{k}-\mathbf{k}'}, \quad (4)$$

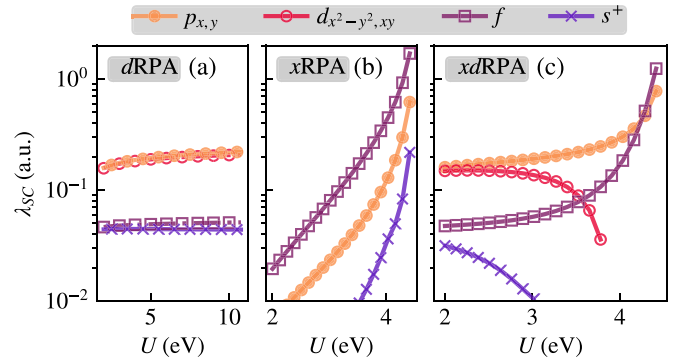


FIG. 4. Competition of superconducting order at the VHS of ABCB for realistic values of the onsite interaction U separated into contribution from spin fluctuations and screening. (a) Screening of long-ranged Coulomb interactions ($dRPA$) favors $p_{x,y}$ ($d_{x^2-y^2,xy}$)-wave order, while f/s^+ order is suppressed for all values of U . (b) Spin-fluctuation exchange ($xRPA$) exclusively promotes spin-triplet f -wave order. (c) Combining screening and spin fluctuations ($xdRPA$) lifts the degeneracy between p/d wave as spin-singlet order is suppressed by ferrimagnetic spin fluctuations. Eventually, f -wave order displaces p -wave order at the Stoner transition.

where $\hat{V}^O(\mathbf{q})$ is the discrete Fourier transform of the Ohno interaction matrix obtained from Eq. (3). Taking only screened Coulomb interactions into account ($dRPA$), the superconducting coupling constant shows two peaks that are located near the VHS and the edge of the valence bands, see Figs. 3(a) and 3(b).

Near the VHS, the leading superconducting order parameter is a doubly degenerate spin triplet with $p_{x,y}$ symmetry that changes sign within each valley as shown in panel (c). The prevalence of $p_{x,y}$ order results from the delicate microscopic competition of inter- vs intravalley scattering: Screening in ABCB selectively enhances intravalley scattering $\mathbf{q}_D \approx \Gamma$ of Cooper pairs, while intervalley scattering $\mathbf{q}_D \approx K^{(\prime)}$ caused by short-ranged terms in the Coulomb interaction is suppressed at the VHS, see Ref. [44]. As the screened interaction $\hat{V}_D^{PP}(\mathbf{k}, \mathbf{k}')$ remains positive in momentum space, promoted order parameters must change sign on the (extended) Fermi surface. Indeed the two spin-triplet $p_{x,y}$ -wave order parameters are accompanied by two spin-singlet $d_{x^2-y^2,xy}$ order parameters with slightly lower coupling constant λ_{SC} as shown in Fig. 4. Meanwhile, f/s^+ -wave order is suppressed near the VHS for realistic values of the onsite U , which contradicts earlier predictions of f/s^+ -wave superconductivity [28,31] based on phenomenological parameters to model intervalley scattering in bi- and tetralayer graphene. The situation for low-hole doping is fundamentally different: As the Fermi surface shrinks to the three-pocket structure shown in Fig. 3, $p_{x,y}$ -wave order is suppressed as an intravalley sign change is increasingly disfavored. Instead, almost degenerate f/s^+ -wave order prevails, which is driven by local interactions as in the $xRPA$ (spin) case. Continuum model studies [34,61] that neglect local interactions contrarily report predominant d -wave SC for low-hole doping, which underlines the importance of considering the full Coulomb interaction with respective ratios of onsite and long-ranged interactions.

Competition of spin and charge fluctuations. Finally, we study the mutual interference of the spin/charge fluctuations

by carrying out independent resummations of (i) short-range interactions in the exchange channel and (ii) long-range interactions in the direct channel ($xdRPA$), see SM [44]. First, we observe that the critical temperature is enhanced reaching $T_c \approx 25$ mK near the Stoner transition as shown in Fig. 3. The order parameter symmetry shows $p_{x,y}$ -wave order near the VHS and f -wave order at the valence band edge reminiscent of the pure screening mechanism. Therefore, spin fluctuations enhance charge fluctuations in the formation of superconductivity in ABCB, especially close to the Stoner transition. Second, the approximate degeneracies between $p_{x,y}/d_{x^2-y^2,xy}$ (f/s^+)-wave order at the VHS (valence band edge) are lifted by ferrimagnetic spin fluctuations as shown in Fig. 4(c). The latter suppress spin-singlet superconductivity such that with increasing U only triplet order parameters with $p_{x,y}$ (f)-wave symmetry prevail. Third, screening of the long-ranged Coulomb tail suppresses local interactions that are essential for spin-fluctuation induced pairing: For larger onsite interactions [$U = 5$ eV, cf. Fig. 3(b)], exchange-driven SC (purple line) is enhanced near the Stoner phase, while the effective coupling constant λ_{SC} within the combined $xdRPA$ approach (orange line) is merely affected. However, directly at the VHS, f -wave SC is recovered before the $xdRPA$ breaks down at the Stoner transition $U \rightarrow U_c$, see Fig. 4(c). We hence argue that methods that account for interchannel feedback, e.g., the functional renormalization group [35,63], could resolve this delicate interplay at the VHS, i.e., eventually suppress the magnetic instability and boost f -wave SC.

Discussion. In this work, we discuss the role of spin fluctuations and screening on the formation of correlated magnetic and superconducting states in tetralayer graphene with emphasis on ABCB stacking. The particular shape and orbital polarization of the bands in ABCB on the hole-doped side resembles the band structure of bilayer graphene in an external electric field. Since ABCB graphene is not topologically obstructed as twisted graphene stacks, we expect our result to be qualitatively transferable to other stacking configurations of few-layer graphene, such as AB

bilayer graphene. In contrast to ABCB, superconductivity in AB graphene emerges at relatively high (experimentally accessible) displacement fields [2–5], implying that ABCB graphene provides an interesting avenue to further stabilize superconductivity in graphene-based multilayers. Due to the metastable nature of ABCB graphene [37], the experimental realization of transport devices is likely to pose special challenges for the sample preparation, especially for the encapsulation of ABCB graphene in hexagonal boron nitride like it is known from ABC trilayer graphene [20,64]. Our results highlight the importance of theoretically studying electronic phases in multilayer graphene stacks with microscopically derived interaction profiles that capture long- and short-ranged Coulomb interactions consistently and motivates further research with orbital-resolved methods that allow for interchannel feedback to faithfully resolve the SC order parameter symmetry at the VHS.

Acknowledgments. We thank C. Stampfer, T. Taubner, and K. Wirth for fruitful discussions. This work was supported by the Excellence Initiative of the German federal and state governments, the Ministry of Innovation of North Rhine-Westphalia and the Deutsche Forschungsgemeinschaft (DFG, German Research Foundation). J.B.P., L.K., A.F., and D.M.K. acknowledge funding by the DFG under RTG 1995, within the Priority Program SPP 2244 “2DMP,” Grant No. 443273985. L.K. and T.O.W. gratefully acknowledge support from the DFG through FOR 5249 (QUAST, Project No. 449872909) and SPP 2244 (Project No. 422707584). T.O.W. is supported by the Cluster of Excellence “CUI: Advanced Imaging of Matter” of the DFG (EXC 2056, Project No. 390715994). D.M.K. acknowledges support by the Max Planck-New York City Center for Nonequilibrium Quantum Phenomena. We acknowledge computational resources provided by the Max Planck Computing and Data Facility, RWTH Aachen University under Projects No. rwth0742 and No. rwth0716, and through the JARA Vergabegremium on the JARA Partition part of the supercomputer JURECA [65] at Forschungszentrum Jülich.

-
- [1] A. M. Seiler, F. R. Geisenhof, F. Winterer, K. Watanabe, T. Taniguchi, T. Xu, F. Zhang, and R. T. Weitz, Quantum cascade of correlated phases in trigonally warped bilayer graphene, *Nature (London)* **608**, 298 (2022).
- [2] H. Zhou, T. Xie, T. Taniguchi, K. Watanabe, and A. F. Young, Superconductivity in rhombohedral trilayer graphene, *Nature (London)* **598**, 434 (2021).
- [3] L. Holleis, C. L. Patterson, Y. Zhang, H. M. Yoo, H. Zhou, T. Taniguchi, K. Watanabe, S. Nadj-Perge, and A. F. Young, Ising superconductivity and nematicity in bernal bilayer graphene with strong spin orbit coupling, [arXiv:2303.00742](https://arxiv.org/abs/2303.00742).
- [4] H. Zhou, L. Holleis, Y. Saito, L. Cohen, W. Huynh, C. L. Patterson, F. Yang, T. Taniguchi, K. Watanabe, and A. F. Young, Isospin magnetism and spin-polarized superconductivity in bernal bilayer graphene, *Science* **375**, 774 (2022).
- [5] Y. Zhang, R. Polski, A. Thomson, É. Lantagne-Hurtubise, C. Lewandowski, H. Zhou, K. Watanabe, T. Taniguchi, J. Alicea, and S. Nadj-Perge, Enhanced superconductivity in spin-orbit proximitized bilayer graphene, *Nature (London)* **613**, 268 (2023).
- [6] F. Winterer, F. R. Geisenhof, N. Fernandez, A. M. Seiler, F. Zhang, and R. T. Weitz, Ferroelectric and anomalous quantum hall states in bare rhombohedral trilayer graphene, [arXiv:2305.04950](https://arxiv.org/abs/2305.04950).
- [7] Y. Cao, V. Fatemi, S. Fang, K. Watanabe, T. Taniguchi, E. Kaxiras, and P. Jarillo-Herrero, Unconventional superconductivity in magic-angle graphene superlattices, *Nature (London)* **556**, 43 (2018).
- [8] M. Yankowitz, S. Chen, H. Polshyn, Y. Zhang, K. Watanabe, T. Taniguchi, D. Graf, A. F. Young, and C. R. Dean, Tuning superconductivity in twisted bilayer graphene, *Science* **363**, 1059 (2019).
- [9] X. Lu, P. Stepanov, W. Yang, M. Xie, M. A. Aamir, I. Das, C. Urgell, K. Watanabe, T. Taniguchi, G. Zhang *et al.*, Superconductors, orbital magnets and correlated states in magic-angle bilayer graphene, *Nature (London)* **574**, 653 (2019).

- [10] Y. Saito, J. Ge, K. Watanabe, T. Taniguchi, and A. F. Young, Independent superconductors and correlated insulators in twisted bilayer graphene, *Nat. Phys.* **16**, 926 (2020).
- [11] P. Stepanov, I. Das, X. Lu, A. Fahimniya, K. Watanabe, T. Taniguchi, F. H. Koppens, J. Lischner, L. Levitov, and D. K. Efetov, Untying the insulating and superconducting orders in magic-angle graphene, *Nature (London)* **583**, 375 (2020).
- [12] M. Oh, K. P. Nuckolls, D. Wong, R. L. Lee, X. Liu, K. Watanabe, T. Taniguchi, and A. Yazdani, Evidence for unconventional superconductivity in twisted bilayer graphene, *Nature (London)* **600**, 240 (2021).
- [13] Y. Cao, D. Rodan-Legrain, J. M. Park, N. F. Yuan, K. Watanabe, T. Taniguchi, R. M. Fernandes, L. Fu, and P. Jarillo-Herrero, Nematicity and competing orders in superconducting magic-angle graphene, *Science* **372**, 264 (2021).
- [14] Y. Zhang, R. Polski, C. Lewandowski, A. Thomson, Y. Peng, Y. Choi, H. Kim, K. Watanabe, T. Taniguchi, J. Alicea *et al.*, Ascendance of superconductivity in magic-angle graphene multilayers, [arXiv:2112.09270](https://arxiv.org/abs/2112.09270).
- [15] J. M. Park, Y. Cao, K. Watanabe, T. Taniguchi, and P. Jarillo-Herrero, Tunable strongly coupled superconductivity in magic-angle twisted trilayer graphene, *Nature (London)* **590**, 249 (2021).
- [16] Y. Cao, J. M. Park, K. Watanabe, T. Taniguchi, and P. Jarillo-Herrero, Pauli-limit violation and re-entrant superconductivity in moiré graphene, *Nature (London)* **595**, 526 (2021).
- [17] H. Kim, Y. Choi, C. Lewandowski, A. Thomson, Y. Zhang, R. Polski, K. Watanabe, T. Taniguchi, J. Alicea, and S. Nadj-Perge, Evidence for unconventional superconductivity in twisted trilayer graphene, *Nature (London)* **606**, 494 (2022).
- [18] X. Liu, N. J. Zhang, K. Watanabe, T. Taniguchi, and J. Li, Isospin order in superconducting magic-angle twisted trilayer graphene, *Nat. Phys.* **18**, 522 (2022).
- [19] D. M. Kennes, M. Claassen, L. Xian, A. Georges, A. J. Millis, J. Hone, C. R. Dean, D. N. Basov, A. N. Pasupathy, and A. Rubio, Moiré heterostructures as a condensed-matter quantum simulator, *Nat. Phys.* **17**, 155 (2021).
- [20] H. Zhou, T. Xie, A. Ghazaryan, T. Holder, J. R. Ehrets, E. M. Spanton, T. Taniguchi, K. Watanabe, E. Berg, M. Serbyn *et al.*, Half-and quarter-metals in rhombohedral trilayer graphene, *Nature (London)* **598**, 429 (2021).
- [21] J. Ahn, S. Park, and B.-J. Yang, Failure of nielsen-ninomiya theorem and fragile topology in two-dimensional systems with space-time inversion symmetry: Application to twisted bilayer graphene at magic angle, *Phys. Rev. X* **9**, 021013 (2019).
- [22] Z. Song, Z. Wang, W. Shi, G. Li, C. Fang, and B. A. Bernevig, All magic angles in twisted bilayer graphene are topological, *Phys. Rev. Lett.* **123**, 036401 (2019).
- [23] L. Zou, H. C. Po, A. Vishwanath, and T. Senthil, Band structure of twisted bilayer graphene: Emergent symmetries, commensurate approximants, and wannier obstructions, *Phys. Rev. B* **98**, 085435 (2018).
- [24] S. Chatterjee, T. Wang, E. Berg, and M. P. Zaletel, Inter-valley coherent order and isospin fluctuation mediated superconductivity in rhombohedral trilayer graphene, *Nat. Commun.* **13**, 6013 (2022).
- [25] A. L. Szabó and B. Roy, Competing orders and cascade of degeneracy lifting in doped bernal bilayer graphene, *Phys. Rev. B* **105**, L201107 (2022).
- [26] A. L. Szabó and B. Roy, Metals, fractional metals, and superconductivity in rhombohedral trilayer graphene, *Phys. Rev. B* **105**, L081407 (2022).
- [27] Y.-Z. You and A. Vishwanath, Kohn-Luttinger superconductivity and intervalley coherence in rhombohedral trilayer graphene, *Phys. Rev. B* **105**, 134524 (2022).
- [28] Z. Li, X. Kuang, A. Jimeno-Pozo, H. Sainz-Cruz, Z. Zhan, S. Yuan, and F. Guinea, Charge fluctuations, phonons and superconductivity in multilayer graphene, *Phys. Rev. B* **108**, 045404 (2023).
- [29] P. A. Pantaleón, A. Jimeno-Pozo, H. Sainz-Cruz, V. T. Phong, T. Cea, and F. Guinea, Superconductivity and correlated phases in non-twisted bilayer and trilayer graphene, *Nat. Rev. Phys.* **5**, 304 (2023).
- [30] T. Cea, P. A. Pantaleón, V. T. Phong, and F. Guinea, Superconductivity from repulsive interactions in rhombohedral trilayer graphene: A Kohn-Luttinger-like mechanism, *Phys. Rev. B* **105**, 075432 (2022).
- [31] A. Jimeno-Pozo, H. Sainz-Cruz, T. Cea, P. A. Pantaleón, and F. Guinea, Superconductivity from electronic interactions and spin-orbit enhancement in bilayer and trilayer graphene, *Phys. Rev. B* **107**, L161106 (2023).
- [32] T. Cea, Superconductivity induced by the intervalley coulomb scattering in a few layers of graphene, *Phys. Rev. B* **107**, L041111 (2023).
- [33] H. Dai, R. Ma, X. Zhang, and T. Ma, Quantum Monte Carlo study of superconductivity in rhombohedral trilayer graphene under an electric field, *Phys. Rev. B* **107**, 245106 (2023).
- [34] A. Ghazaryan, T. Holder, E. Berg, and M. Serbyn, Multilayer graphenes as a platform for interaction-driven physics and topological superconductivity, *Phys. Rev. B* **107**, 104502 (2023).
- [35] W. Qin, C. Huang, T. Wolf, N. Wei, I. Blinov, and A. H. MacDonald, Functional renormalization group study of superconductivity in rhombohedral trilayer graphene, *Phys. Rev. Lett.* **130**, 146001 (2023).
- [36] G. Wagner, Y. H. Kwan, N. Bultinck, S. H. Simon, and S. Parameswaran, Superconductivity from repulsive interactions in bernal-stacked bilayer graphene, [arXiv:2302.00682](https://arxiv.org/abs/2302.00682).
- [37] K. G. Wirth, J. B. Hauck, A. Rothstein, H. Kyoseva, D. Siebenkotten, L. Conrads, L. Klebl, A. Fischer, B. Beschoten, C. Stampfer, D. M. Kennes, L. Waldecker, and T. Taubner, Experimental observation of ABCB stacked tetralayer graphene, *ACS Nano* **16**, 16617 (2022).
- [38] S. S. Atri, W. Cao, B. Alon, N. Roy, M. V. Stern, V. Falko, M. Goldstein, L. Kronik, M. Urbakh, O. Hod, and M. B. Shalom, Spontaneous electric polarization in graphene polytypes, [arXiv:2305.10890](https://arxiv.org/abs/2305.10890).
- [39] Y.-Z. Chou, F. Wu, J. D. Sau, and S. Das Sarma, Acoustic-phonon-mediated superconductivity in bernal bilayer graphene, *Phys. Rev. B* **105**, L100503 (2022).
- [40] Y.-Z. Chou, F. Wu, and S. Das Sarma, Enhanced superconductivity through virtual tunneling in bernal bilayer graphene coupled to WSe₂, *Phys. Rev. B* **106**, L180502 (2022).
- [41] Y.-Z. Chou, F. Wu, J. D. Sau, and S. Das Sarma, Acoustic-phonon-mediated superconductivity in moiréless graphene multilayers, *Phys. Rev. B* **106**, 024507 (2022).
- [42] A. Grüneis, C. Attaccalite, L. Wirtz, H. Shiozawa, R. Saito, T. Pichler, and A. Rubio, Tight-binding description of the

- quasiparticle dispersion of graphite and few-layer graphene, *Phys. Rev. B* **78**, 205425 (2008).
- [43] M. Aoki and H. Amawashi, Dependence of band structures on stacking and field in layered graphene, *Solid State Commun.* **142**, 123 (2007).
- [44] See Supplemental Material at <http://link.aps.org/supplemental/10.1103/PhysRevResearch.6.L012003> for details on the non-interacting Hamiltonian, random phase approximation for magnetic and superconducting order for different parameter choices, and explanations of the χ RPA, d RPA, and χd RPA mechanisms.
- [45] K. G. Wirth, H. Linnenbank, T. Steinle, L. Banszerus, E. Icking, C. Stampfer, H. Giessen, and T. Taubner, Tunable s -SNOM for nanoscale infrared optical measurement of electronic properties of bilayer graphene, *ACS Photonics* **8**, 418 (2021).
- [46] A. McEllistrim, A. Garcia-Ruiz, Z. A. H. Goodwin, and V. I. Fal'ko, Spectroscopic signatures of tetralayer graphene polytypes, *Phys. Rev. B* **107**, 155147 (2023).
- [47] A. Garcia-Ruiz, V. Enaldiev, A. McEllistrim, and V. I. Fal'ko, Mixed-stacking few-layer graphene as an elemental weak ferroelectric material, *Nano Lett.* **23**, 4120 (2023).
- [48] L. Klebl and C. Honerkamp, Inherited and flatband-induced ordering in twisted graphene bilayers, *Phys. Rev. B* **100**, 155145 (2019).
- [49] C. Huang, T. M. R. Wolf, W. Qin, N. Wei, I. V. Blinov, and A. H. MacDonald, Spin and orbital metallic magnetism in rhombohedral trilayer graphene, *Phys. Rev. B* **107**, L121405 (2023).
- [50] T. O. Wehling, E. Şaşıoğlu, C. Friedrich, A. I. Lichtenstein, M. I. Katsnelson, and S. Blügel, Strength of effective coulomb interactions in graphene and graphite, *Phys. Rev. Lett.* **106**, 236805 (2011).
- [51] M. Rösner, E. Şaşıoğlu, C. Friedrich, S. Blügel, and T. O. Wehling, Wannier function approach to realistic coulomb interactions in layered materials and heterostructures, *Phys. Rev. B* **92**, 085102 (2015).
- [52] J. Nilsson, A. H. Castro Neto, N. M. R. Peres, and F. Guinea, Electron-electron interactions and the phase diagram of a graphene bilayer, *Phys. Rev. B* **73**, 214418 (2006).
- [53] E. V. Castro, N. M. R. Peres, T. Stauber, and N. A. P. Silva, Low-density ferromagnetism in biased bilayer graphene, *Phys. Rev. Lett.* **100**, 186803 (2008).
- [54] D. J. Scalapino, A common thread: The pairing interaction for unconventional superconductors, *Rev. Mod. Phys.* **84**, 1383 (2012).
- [55] S. Graser, T. Maier, P. Hirschfeld, and D. Scalapino, Near-degeneracy of several pairing channels in multiorbital models for the Fe pnictides, *New J. Phys.* **11**, 025016 (2009).
- [56] A. Fischer, Z. A. Goodwin, A. A. Mostofi, J. Lischner, D. M. Kennes, and L. Klebl, Unconventional superconductivity in magic-angle twisted trilayer graphene, *npj Quantum Mater.* **7**, 5 (2022).
- [57] A. Fischer, L. Klebl, C. Honerkamp, and D. M. Kennes, Spin-fluctuation-induced pairing in twisted bilayer graphene, *Phys. Rev. B* **103**, L041103 (2021).
- [58] J. González and T. Stauber, Kohn-Luttinger superconductivity in twisted bilayer graphene, *Phys. Rev. Lett.* **122**, 026801 (2019).
- [59] J. Gonzalez and T. Stauber, Universal mechanism of Ising superconductivity in twisted bilayer, trilayer and quadrilayer graphene, [arXiv:2303.00583](https://arxiv.org/abs/2303.00583).
- [60] S. Raghu, S. A. Kivelson, and D. J. Scalapino, Superconductivity in the repulsive hubbard model: An asymptotically exact weak-coupling solution, *Phys. Rev. B* **81**, 224505 (2010).
- [61] A. Ghazaryan, T. Holder, M. Serbyn, and E. Berg, Unconventional superconductivity in systems with annular fermi surfaces: Application to rhombohedral trilayer graphene, *Phys. Rev. Lett.* **127**, 247001 (2021).
- [62] K. Ohno, Some remarks on the Pariser-Parr-Pople method, *Theor. Chim. Acta* **2**, 219 (1964).
- [63] W. Metzner, M. Salmhofer, C. Honerkamp, V. Meden, and K. Schönhammer, Functional renormalization group approach to correlated fermion systems, *Rev. Mod. Phys.* **84**, 299 (2012).
- [64] Y. Yang, Y.-C. Zou, C. R. Woods, Y. Shi, J. Yin, S. Xu, S. Ozdemir, T. Taniguchi, K. Watanabe, A. K. Geim, K. S. Novoselov, S. J. Haigh, and A. Mishchenko, Stacking order in graphite films controlled by van der Waals technology, *Nano Lett.* **19**, 8526 (2019).
- [65] P. Thörnig, JURECA: Data centric and booster modules implementing the modular supercomputing architecture at Jülich supercomputing centre, *Journal of large-scale research facilities JLSRF* **7**, A182 (2021).